RSC Advances

PAPER

View Article Online
View Journal | View Issue

Cite this: *RSC Adv.*, 2021, **11**, 30918

A microporous Ce-based MOF with the octahedron cage for highly selective adsorption towards xenon over krypton†

Xiaoling Wu,[ab] Zi-Jian Li,[ab] He Zhou,[ab] Lin Li,[ab] Zhenghua Qian,[a] Nan Qian,[a] Xinxin Chu*[ab] and Wei Liu*[ab]

Received 22nd June 2021
Accepted 25th August 2021

DOI: 10.1039/d1ra04824d

rsc.li/rsc-advances

The collection of high-purity noble gases with recyclable nuclides provides substantial economic benefits and minimizes the risk of environmental pollution, which is a future development tendency for nuclear industries. Here, **Ce-SINAP-1**, with its radiation-resistance (up to 20 kGy of γ-ray irradiation) and suitable pore channels for the separation of noble gases (Ar, Kr and Xe), was synthesized. **Ce-SINAP-1** exhibited the selective adsorption of Xe (2.02 mmol g^{-1}) over Kr (0.67 mmol g^{-1}) and Ar (0.27 mmol g^{-1}) at 293 K (1 bar) with a Henry's selectivity of 8.24 (Xe/Kr), and an ideal adsorbed solution theory selectivity of 14.9 (Xe : Kr 20 : 80). The result of the dynamic breakthrough experiment also indicates a good separation for Xe/Kr with Ar.

Introduction

Xenon and krypton are essential sources applied in the industrial and medical fields, such as imaging, anesthesia and lighting in traffic systems.[1–4] However, the collection and purification of xenon and krypton from air through cryogenic distillation and membrane separation are expensive.[5,6] The recycling and storage of effluent radioactive noble gases from nuclear reactors and reprocessing plants are new approaches for sustainable development, which can mitigate air pollution problems and reduce health risks.[7,8] Porous materials as modified zeolites and activated carbons have been extensively used in nuclear infrastructure for radioactive noble gas treatment due to their economical character and easy-operability.[9,10] While those materials cannot reach a high Xe/Kr separation, the selectivity approximately ranges from four to six.[11–14]

Metal–organic frameworks (MOFs) with multifarious chemical functionalities, tunable pore sizes, high porosity, and various topological structures, have undergone rapid development, providing substantial advantages in applications such as catalysis, gas storage and purification.[15–20] Studies on the separation of natural gases, such as CH_4, C_2H_2 and iodine vapor using MOFs have drawn considerable attention.[21–25] Furthermore, studies on the selectivity of Xe/Kr with MOFs under irradiation conditions have emerged with the development of nuclear energy.[26–39] Thallapally *et al.* proposed a concept of a two-bed radioactive off-gas treatment with Ni/DOBDC and FMOF-Cu.[40,41] Sameh *et al.* synthesized a SIFSIX-3-M (Cu, Zn, Co, Fe, Ni) series. SIFSIX-3-Cu showed a dynamic selectivity of 4.81 with Xe/Kr and 24.38 with Kr/N_2 in dry air, which could endure 50 kGy β and γ irradiation.[42,43] Yan *et al.* reported a series of Zr-Fum MOF and UiO-66(Zr), the Zr-Fum-Me possessed a Henry's selectivity of 14.8 with a dose of 8 kGy γ-ray irradiation resistant, UiO-66(Zr) owns a similar structure to that of Zr-Fum with a Xe/Kr selectivity of 7.7 and 2 kGy γ irradiation resistance.[44,45]

Cerium is a rare-earth metal in the lanthanide class possessing advantages of affordability and accessibility in nature. Cerium is one of the typical nuclides and it is planed to remove from the radioactive waste solution of nuclear facilities as the target object with the sorption method.[46–48] Alternatively, the removable cerium can be recycled and reutilized in some ways rather than treated as solid waste. In this study, Ce(IV) and an organic ligand (4,4′,4″,4‴-methanetetrayltetrabenzoic acid, H_4MTB) with a tetrahedral geometry were synthesized as MOF adsorbents, namely **Ce-SINAP-1** (SINAP = Shanghai Institute of Applied Physics), to extend its application in the separation of noble gases (Ar, Kr, Xe; Ar as the carrier gas that flows into the reactor core vessel and purge Kr and Xe to the off-gas treatment system). The coordination geometric features and high coordination numbers indicate that cerium-based organic frameworks possess great stability in coordination geometries than several other transition and alkaline earth metals. In addition, irradiation experiments were conducted with **Ce-SINAP-1** to confirm its stability in the off-gas treatment system of

[a]*Shanghai Institute of Applied Physics, Chinese Academy of Sciences, Shanghai 201800, China. E-mail: liuwei@sinap.ac.cn; chuxinxin@sinap.ac.cn*

[b]*University of Chinese Academy of Sciences, Beijing 100049, China*

† Electronic supplementary information (ESI) available: PXRD, TGA, BET and flowchart of the dynamic breakthrough curve. CCDC 2085724. For ESI and crystallographic data in CIF or other electronic format see DOI: 10.1039/d1ra04824d.

a Thorium-based Molten Salt Reactor with liquid fuel (TMSR-LF) designed by SINAP, Chinese Academy of Sciences (CAS).

Experimental section

Materials

All chemicals purchased from commercial suppliers were used without additional purification. Ceric nitrate ($Ce(NO_3)_4$) (99.9%, Shanghai Macklin Biochemical Co., Ltd.), *n*-hexane ($CH_3(CH_2)_4CH_3$) (97%, Shanghai Macklin Biochemical Co., Ltd), 4,4′,4″,4‴-methanetetrayl-tetra benzoic acid (H_4MTB) (98%, Jilin Chinese Academy of Sciences – Yanshen Technology Co., Ltd.), *N*,*N*′-dimethylformamide (DMF, $(CH_3)_2HCON$) (≥99.0%, Sinopharm Chemical Reagent Co., Ltd.), acetic acid (CH_3COOH) (≥99.5%, Sinopharm Chemical Reagent Co., Ltd.).

Synthesis of Ce-SINAP-1

Organic ligand H_4MTB ($C_{29}H_{20}O_8$, 15.9 mg, 0.032 mmol) and $Ce(NO_3)_4$ (12.4 mg, 0.032 mmol) was dissolved in 2.8 mL of DMF, and then, 0.24 mL of CH_3COOH was added in the solution under homogeneous mixing. Next, the mixture liquid was transferred into a 10 mL Teflon-lined stainless-steel vessel and mechanically sealed. With an effective heating time (24 h) and heating temperature (393 K), the vessel was allowed to move from the oven and was cooled down at room temperature. White transparent crystals were obtained and cleaned with DMF several times to remove the unreacted ligands. Yield, 70.6% according to H_4MTB.

Characterizations

Single crystal X-ray diffraction (SCXRD). The **Ce-SINAP-1** data were collected using a Bruker D8-Venture single-crystal X-ray diffractometer (Mo Kα radiation, $\lambda = 0.71073$ Å). The structure was solved using intrinsic phasing with the ShelXT[49] structure solution program, and refined using the least squares minimization with the ShelXL[50] refinement package in Olex2.[51] The SQUEEZE routine in PLATON was used to remove highly disordered solvent species in the voids. The crystallographic data of **Ce-SINAP-1** are presented in Table S1.† The selected bond lengths and angles are presented in Table S2.†

Powder X-ray diffraction (PXRD). PXRD analyses were conducted using a Bruker D8 Advance diffractometer with an image detector and Cu Kα radiation ($\lambda = 1.5418$ Å) X-ray generator operating at 40 kV and 40 mA. Data were collected at a rotation rate of 2.0 ° min^{-1} in the range of measurement from 5° to 40° at room temperature in continuous PSD fast scan mode.

Thermogravimetric analysis (TGA). Thermogravimetric analysis was conducted in N_2 atmosphere at a heating rate of 10 °C min^{-1} from 25 °C to 750 °C by using a NETZSCH STA 449C Jupiter thermal analyzer.

Stability tests

γ-Ray irradiation resistance measurements. γ-Ray irradiation tests were performed using a ^{60}Co irradiation source (2.22×10^{15} Bq). All irradiation tests were conducted at ambient temperature.

Gas adsorption measurements

Before gas sorption measurements, approximately 40 mg of samples were filtered and transferred in *n*-hexane for 6 h to exchange the high boiling point guest solvent in the pores. *N*-Hexane was used as the low boiling point and low surface tension solvent that could optimize the activation process and pore volume occupied by the high boiling point guest solvent. The samples were pretreated in a quartz vessel by mechanical and molecular pump under high vacuum conditions (<1.0 Pa) for 12 h under continuous heating at 393 K.

N_2 and noble gas sorption curves were analyzed by an ASAP 2020 surface characterization analyzer from Micromeritics Instruments Corporation with ultra-high purity gases from Air Liquid Company and Newradar special gas company (He, Ar, Kr, Xe and N_2; >99.999%). N_2 sorption experiments were carried out at 77 K in a liquid nitrogen bath. Noble gas isotherms were obtained at 273 K, 293 K and 313 K using a cooled Dewar, respectively. The isothermal points and Brunauer–Emmett–Teller specific surface area (BET) were analyzed through the ASAP 2020 software.

Gas breakthrough experiments

Before the dynamic breakthrough experiment, approximately 0.5 g of activated **Ce-SINAP-1** samples (*n*-hexane solvent exchanged and effectively heated at 393 K under high-vacuum conditions for 12 h) were packed into a stainless-steel column (length: 20 cm, φ 4 mm) with silica wool filling at both ends, which was swept with 10 mL min^{-1} helium gas for two hours at 393 K. During the experiment, a test gas (5 ppm of Kr, 50 ppm of Xe, >99.999% Ar) flowed into the packed bed at 293 K at a rate of 2 mL min^{-1} in a temperature-controlled chamber. A Shimadzu 2014 gas chromatograph was used for the gas concentration measurement. A flow controller (Kofloc 8500, 0–20 mL min^{-1}), gas mixture (AMETEK MGB1000) and pressure gauges (Fluke, 0.00–100 kPa) were equipped in the test platform of dynamic sorption. (Fig. S14†).

Results and discussion

Ce-SINAP-1 (Ce(MTB) $(C_3H_7NO_5)_4(H_2O)_5$) was obtained through the solvothermal reaction with the mixture of H_4MTB, $Ce(NO_3)_4$ and CH_3COOH solved in a DMF solution in a mechanical sealed vessel under the 393 K effective heating condition for 24 h. The single crystal X-ray diffractogram reveals that **Ce-SINAP-1** was in a triclinic crystal system and had the $P\bar{1}$ space group. One asymmetric single unit is composed of one Ce^{4+} ion, one MTB^{4-} ligand and six O^{2-}. H_4MTB lost its four protons to form MTB^{4-}, whose O atoms were all combined to Ce^{4+} as the point of junction. Each Ce^{4+} center was surrounded by eight O atoms including six O atoms from three bidentate carboxylate groups and two O atoms from two monodentate carboxylate groups, which formed a trigonal tetrakaidekahedron coordination geometry. Two CeO_8 formed binary clusters, which served as connected nodes for constructing a 3D framework (Fig. 1a, d and S1†). The eight MTB^{4-} ligands and six CeO_8 binary clusters generated an octahedron cage with a size of

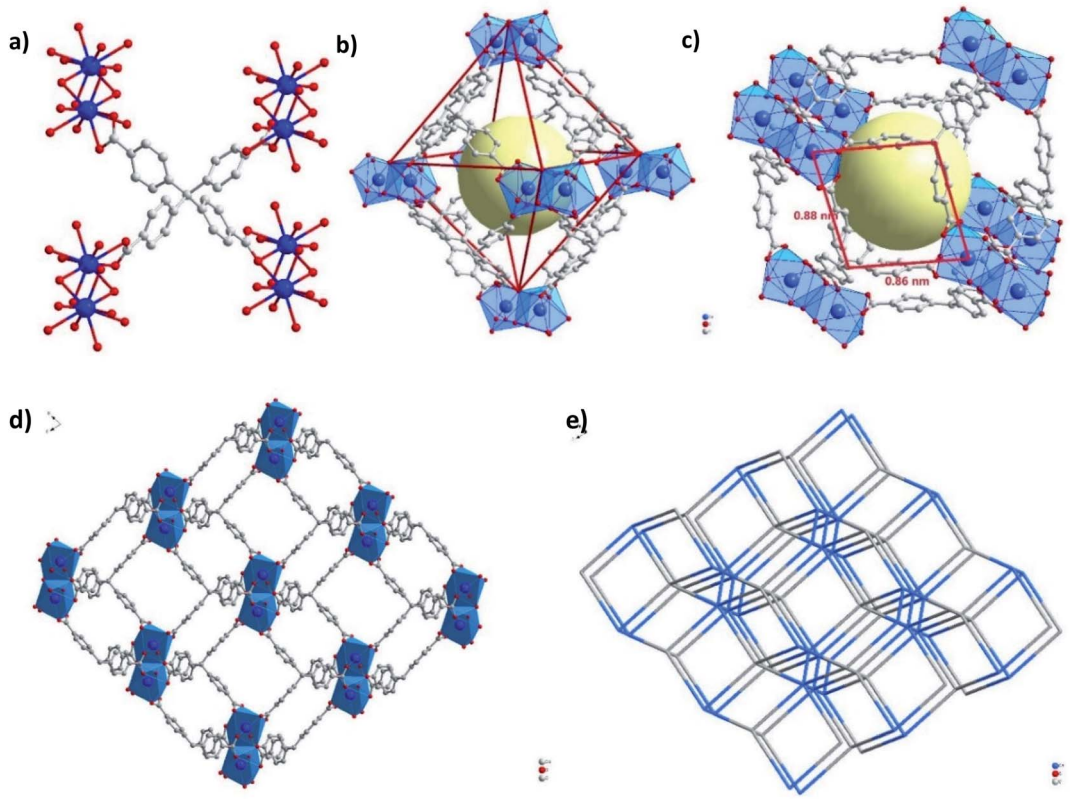

Fig. 1 (a) The coordination of the tetrahedral ligand. (b) The rhombohedral windows. (c) The octahedron cage. (d) The 3D porous structure of **Ce-SINAP-1**. (e) The simplified topological net of **Ce-SINAP-1**.

approximately 25.8 Å × 21.0 Å × 21.2 Å according to the distances of opposite vertices (Fig. 1b). The solvent accessible volume in the fully evacuated **Ce-SINAP-1** was about 58.6% estimated by PLATON. It revealed that with an effective activation process, the volume of cages was available to accommodate Xe, Kr and Ar atoms. The rhombohedral windows connected to the cages with an approximate size of ~8.6 Å × 8.8 Å (Ce1–C and C–Ce1a, respectively), which functionalized the separation and transport of noble gases due to the dynamic diameter (Fig. 1c). As the Xe/Kr selectivity and adsorption capacity were correlated to the geometric properties, the size of the channel approximately from 4.1–8 Å (dynamic diameter of Xe: 4.1 Å) (Fig. S7†) was accessible for the Xe adsorption and separation among the noble gases.[52–54]

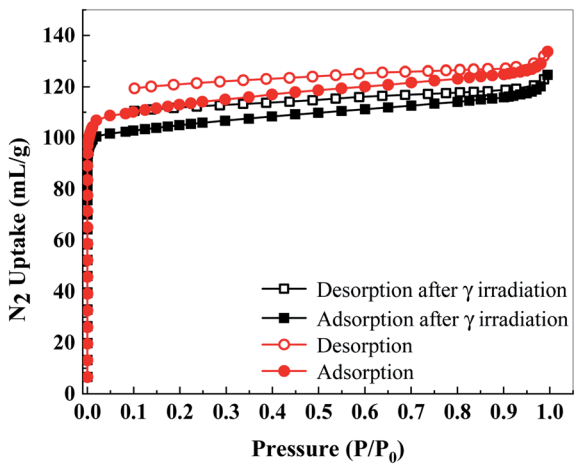

Fig. 2 N_2 adsorption (solid dot)/desorption (hollow dot) isotherms for the activated **Ce-SINAP-1** samples at 77 K before and after the γ-ray irradiation.

TGA was conducted at 25–750 °C under N_2 atmosphere for the as-synthesized samples and samples after activation (Fig. S3†). The 33.61% loss of weight from 30 °C to 260 °C may be attributed to the water and high-boiling solvent DMF in the pores of the samples. The activated sample did not lose much weight from 30 °C to 250 °C, and it showed that the activation process almost made the sample free of the guest solvent. The downtrend of both curves reveals that the structure probably began to collapse to some extent. The resultant structure was totally damaged until 550 °C.

The PXRD analysis indicated that the patterns of the as-synthesized samples were consistent with the simulated one. Moreover, **Ce-SINAP-1** retained its structure under the activation process and ionizing radiation (γ-ray irradiation) after total doses of 20 kGy (Fig. S4†). The *in situ* PXRD analysis was conducted under N_2 atmosphere from 150 °C to 450 °C. The material kept a good crystal structure under 250 °C. When the temperature reached 350 °C, the characteristic peaks weakened, which revealed that the crystal began to collapse. When the temperature rose to 450 °C, the characteristic peaks almost

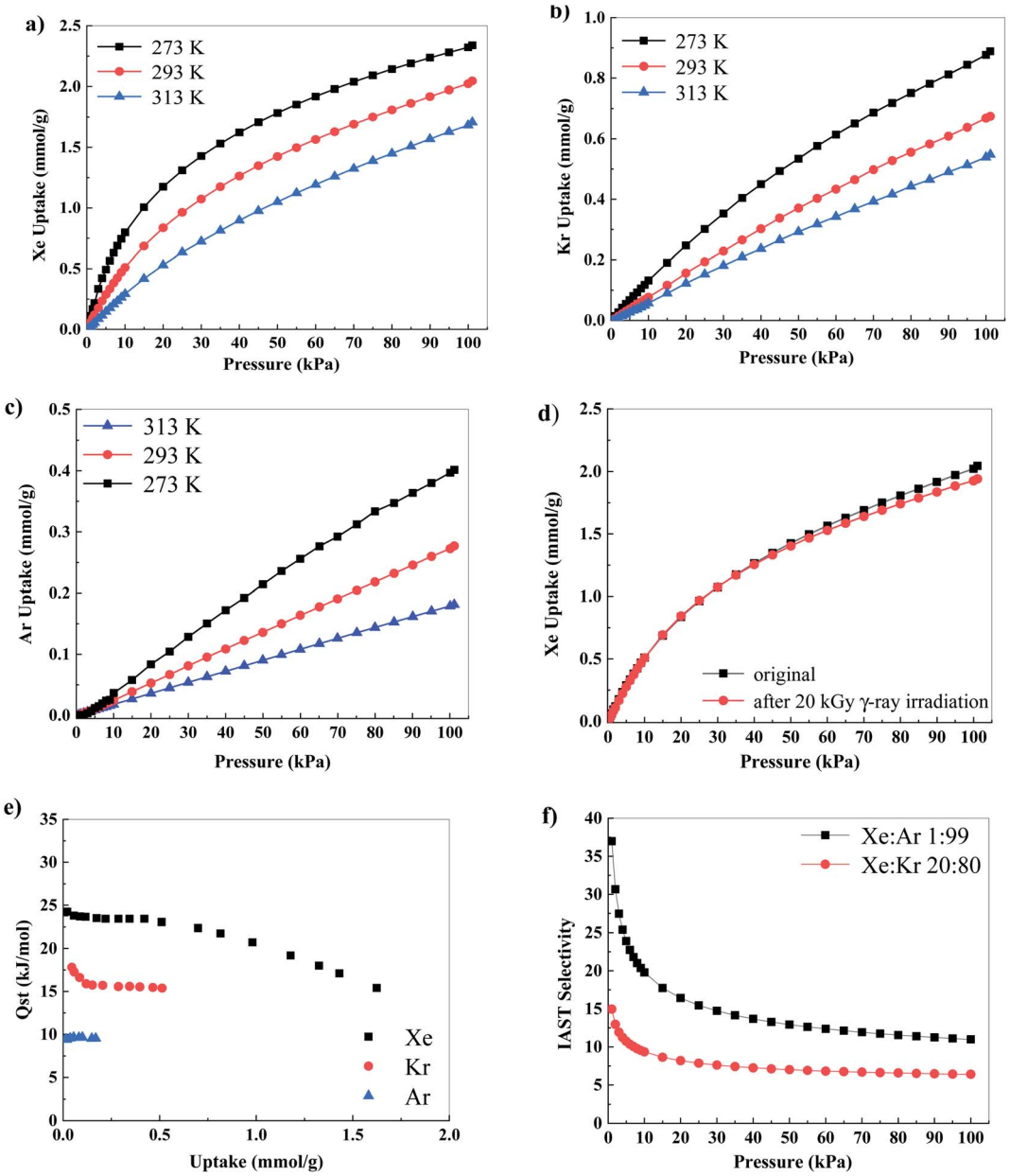

Fig. 3 (a) Xe adsorption isotherms for **Ce-SINAP-1** at 273 K, 293 K and 313 K. (b) Kr adsorption isotherms for **Ce-SINAP-1** at 273 K, 293 K and 313 K. (c) Ar adsorption isotherms for **Ce-SINAP-1** at 273 K, 293 K and 313 K. (d) Xe adsorption isotherms for **Ce-SINAP-1** at 293 K before and after 20 kGy of γ-ray irradiation. (e) The isosteric heat of adsorption (Q_{st}) values of Xe, Kr and Ar calculated from adsorption isotherms on **Ce-SINAP-1** from 273–313 K. (f) Calculated IAST selectivity for a binary Xe/Kr mixture (v/v = 20/80) and Xe/Ar mixture (v/v = 1/99) of **Ce-SINAP-1** at 293 K.

disappeared, which revealed that a phase change occurred in the crystal and the structure collapsed (Fig. S5†).

The porosity character of the framework was analyzed through N_2 sorption experiments at 77 K in a liquid nitrogen bath. A typical type-I adsorption isothermal curve and an apparent BET surface area of 459.4 $m^2\ g^{-1}$ were obtained, which exhibited microporous characteristics of **Ce-SINAP-1**. The N_2 uptake capacity was 134.7 and 124.7 mL g^{-1} before and after γ-ray irradiation at 77 K ($P/P_0 = 1$) (Fig. 2). The BET of **Ce-SINAP-1** after 20 kGy of γ-ray irradiation was 431.9 $m^2\ g^{-1}$, slightly lower than that before the γ-ray irradiation (Fig. S6†). These results indicated that **Ce-SINAP-1** is a sufficient adsorbent candidate for the radioactive off-gas treatment of nuclear facilities. The pore size distribution of **Ce-SINAP-1** ranged from 0.46 to 1.04 nm (Fig. S7†), which nearly corresponded to the single-crystal structure.

Single-component sorption isotherms (including adsorption and desorption isotherms) of noble gases (Xe, Kr and Ar) were obtained under 273 K, 293 K and 313 K in the pressure range from 0 to 100 kPa (Fig. 3a–c, S8–S10†). The three noble gases adsorption isothermal curves presented a single-site Langmuir–Freundlich profile with a steep slope at low pressures (Table

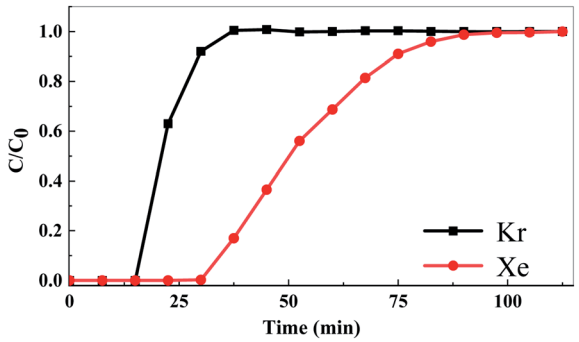

Fig. 4 Breakthrough curves with Ce-SINAP-1 under mixture gas (Kr, Xe, Ar) at 293 K and 1 atm.

S3†). At 100 kPa, **Ce-SINAP-1** demonstrated Xe adsorption capacities of 2.32, 2.02 and 1.68 mmol g^{-1} at 273 K, 293 K and 313 K, respectively. Kr and Ar uptake capacity were 0.68 and 0.27 mmol g^{-1} at 293 K and 100 kPa. The Xe uptake was three times higher than Kr at 293 K, which revealed that the adsorption affinity was stronger between the material and Xe. Beside the N_2 sorption and BET tests, the Xe isothermal curve was another way to prove the radiotolerance of the material. The Xe uptake curve after 20 kGy of γ-ray irradiation was consistent with the original samples (Fig. 3d).

The isosteric heat of adsorption (Q_{st}) was calculated using the Clausius–Clapeyron equation to evaluate the adsorption affinity between the noble gases and the MOF according to the isothermal curves at three different temperatures. The Q_{st} value of Xe near zero-coverage for **Ce-SINAP-1** was estimated to be 24.2 kJ mol^{-1}, higher than those of Kr (17.8 kJ mol^{-1}) and Ar (9.4 kJ mol^{-1}) (Fig. 3e). Therefore, the isosteric heat of adsorption values indicated that the extent of attraction for Xe in this material was stronger than those for Kr and Ar at low pressures.

Henry's constant represents the partition of the adsorbate between its bulk phase and adsorbed phase at low pressures according to the slope of the isothermal curves; it is used to evaluate the selectivity among various noble gases.[55] Henry's constants for **Ce-SINAP-1** were 6.76, 0.82 and 0.23 mmol g^{-1} bar^{-1} for Xe, Kr and Ar at 293 K, respectively. The Xe/Kr selectivity based on Henry's constants was 8.2 (Fig. S11–S13, Table S4†), higher than that reported for typical porous materials (*e.g.*, UiO-66).

The basis of single-component noble gas adsorption isothermal curves, ideal adsorbed solution theory (IAST) was used to determine the Xe/Kr and Xe/Ar selectivity. The IAST Xe/Kr selectivity of **Ce-SINAP-1** for a 20 : 80 Xe : Kr and 1 : 99 Xe : Ar binary gas mixture at 293 K were 14.9 and 36.9 at low pressure loading, respectively (Fig. 3f).

The dynamic adsorption with ternary gases was performed to moderate the off-gas treatment condition in TMSR-LF. Argon was used as the carrier gas, and the radioactive Kr and Xe were swept from the reactor to the off-gas treatment system. The breakthrough experiment was conducted using a gas mixture (5 ppm Kr, 50 ppm Xe, and Ar > 99.999%) at 293 K at a total flow rate of 2 mL min^{-1}. The concentration of Kr was first recorded by a pulsed discharge detector (PDD) in the gas chromatograph after 23 min, and Xe began to elute through the packed bed until 35 min (Fig. 4), indicating a high Xe/Kr separation in the argon atmosphere through **Ce-SINAP-1**.

The interaction between the MOF and Xe was due to several main factors, including the entrance size and inner volume of the pores, the open-metal sites and polar groups as –O and –OH. Beside the experimental results, the state density of Xe in **Ce-SINAP-1** was used to explain the interaction among those elements in the structure (Fig. S15†). The state density signal of Xe in **Ce-SINAP-1** arose in the energy range from 5 to 7 eV, which was dominantly contributed by C atoms and secondly by Ce atoms. C atoms and Ce atoms are the main parts of the framework of **Ce-SINAP-1** including the pore entrance and cages. The lack of open-metal sites and extra polar-groups prompted the narrow entrance window of **Ce-SINAP-1** functionalizing as a sieve for noble gases with different dynamic diameters by the van der Waals force.

Conclusions

A novel MOF **Ce-SINAP-1** was synthesized, which exhibited a satisfactory performance in the adsorption and separation of Xe over Kr and Ar. The Xe uptake was 2.02 mmol g^{-1} at 293 K under 100 kPa. The Henry's selectivity of Xe/Kr and Xe/Ar were 8.24 and 29.39 at 293 K, respectively. This performance could be attributed to the narrow windows and pore volume in this framework. Moreover, **Ce-SINAP-1** exhibited a favorable γ-ray radiation resistance with 20 kGy, suggesting that it can be a competitive candidate for the removal and recycling of radioactive Xe in the off-gas treatment systems of nuclear power plants.

Conflicts of interest

There are no conflicts to declare.

Acknowledgements

We are grateful for the support provided by National Natural Science Foundation of China (No. 51606210 and 21906163), Young Potential Program of Shanghai Institute of Applied Physics, Chinese Academy of Sciences (No. YX2019007) and the Youth Innovation Promotion Association, Chinese Academy of Sciences (Grant No. 2021254).

References

1 G. A. Lane, M. L. Nahrwold, A. R. Tait, M. Taylor-Busch, P. J. Cohen and A. R. Beaudoin, Anesthetics as teratogens: nitrous oxide is fetotoxic, xenon is not, *Science*, 1980, **210**, 899–901.
2 L. Liu, Y. Xu and P. Tang, Mechanistic insights into xenon inhibition of NMDA receptors from MD simulations, *J. Phys. Chem. B*, 2010, **114**, 9010–9016.
3 F. G. Kerry *Industrial Gas Handbook: Gas Separation and Purification.* CRC Press, Boca Raton Florida. 2007.

4 R. T. Yang *Gas separation by adsorption process;* Butterworth-Heinemann, 2013.
5 R. S. Nick, G. G. Troy, R. G. Mitchell, D. L. Jack, J. Robert, M. S. Denis and K. T. Praveen, Radioactive Iodine and Krypton Control for Nuclear Fuel Reprocessing Facilities, *Sci. Technol. Nucl. Install.*, 2013, 1–12.
6 D. Banerjee, C. M. Simon, S. K. Elsaidi, M. Haranczyk and P. K. Thallapally, Xenon gas separation and storage using metal–organic frameworks, *Chem*, 2018, **4**, 466–494.
7 J. P. Fontaine, F. Pointurier, X. Blanchard and T. Taffary, Atmospheric xenon radioactive isotope monitoring, *J. Environ. Radioact.*, 2004, **72**, 129–135.
8 K. R. Smith, H. Frumkin, K. Balakrishnan, C. D. Butler, Z. A. Chafe, I. Fairlie, P. Kinney, T. Kjellstrom, D. L. Mauzerall, T. E. McKone, A. J. McMichael and M. Schneider, Energy and human health, *Annu. Rev. Public Health*, 2013, **34**, 159–188.
9 R. T. Yang *Adsorbents: Fundamentals and Applications*. John Wiley&Sons Inc., Hoboken. 2003.
10 J. Izumi Waste gas treatment using zeolites in nuclear-related industries, *Handbook of Zeolites Science and Technology*, ed. S. M. Auerbach, K. A. Carrodo and P. K. Dutta, Marcel Dekker, New York. 2003.
11 C. J. Jameson, A. K. Jameson and H.-M. Lim, Competitive adsorption of xenon and krypton in zeolite NaA: ^{129}Xe nuclear magnetic resonance studies and grand cannonical monte carlo simulation, *J. Chem. Phys.*, 1997, **107**, 4364–4372.
12 K. Munakata, K. Tanaka, S. Yamatsuki, T. Fukumatsu, S. Kanjo, Y. Yokoyama and M. Nishikawa, Dynamic of adsorption of Kr and Xe on MS5A and activated charcoal, *J. Nucl. Sci. Technol.*, 2001, **34**, 853–861.
13 C. G. Saxton, A. Kruth, M. Castro, P. A. Wright and R. F. Howe, Xenon adsorption in synthetic chabazite zeolites, *Microporous Mesoporous Mater.*, 2010, **129**, 68–73.
14 R. E. Bazan, M. Bastos-Neto, A. Moeller, F. Dreisbach and R. Staudt, Adsorption equilibria of O_2, Ar, Kr and Xe on activated carbon and zeolites: single component and mixture data, *Adsorption*, 2011, **17**, 371–383.
15 W. G. Cui, T. L. Hu and X. H. Bu, Metal–organic framework materials for the separation and purification of light hydrocarbons, *Adv. Mater.*, 2020, **32**, 1806445.
16 K. Tan, S. Jensen, S. Zuluaga, E. K. Chapman, H. Wang, R. Rahman, J. Cure, T. H. Kim, J. Li, T. Thonhauser and Y. J. Chabal, Role of hydrogen bonding on transport of coadsorbed gases in metal–organic frameworks materials, *J. Am. Chem. Soc.*, 2018, **140**, 856–859.
17 Z. Shi, Y. Tao, J. Wu, C. Zhang, H. He, L. Long, Y. Lee, T. Li and Y.-B. Zhang, Robust metal-triazolate frameworks for CO_2 capture from flue gas, *J. Am. Chem. Soc.*, 2020, **142**, 2750–2754.
18 X.-W. Liu, Y.-M. Gu, T.-J. Sun, Y. Guo, X.-L. Wei, S.-S. Zhao and S.-D. Wang, Water resistant and flexible MOF materials for highly efficient separation of methane from nitrogen, *Ind. Eng. Chem. Res.*, 2019, **58**, 20391–20400.
19 J. L. C. Rowsell and O. M. Yaghi, Metal–organic frameworks: a new class of porous materials, *Microporous Mesoporous Mater.*, 2004, **73**, 3–14.
20 G. Férey, Hybrid porous solids: past, present, future, *Chem. Soc. Rev.*, 2008, **37**, 191–214.
21 B. Safarkoopayeh, A. Abbasi and A. Shayesteh, Two new metal–organic frameworks: synthesis, characterization, gas adsorption and simulation, *Inorg. Chem. Commun.*, 2021, **127**, 108502.
22 F. Hu, Z. Di, M. Wu and J. Li, Building a robust 3D Ca-MOF by a new square Ca_4O SBU for purification of natural gas, *Dalton Trans.*, 2020, **49**, 8836.
23 Li. Liu, Z. Yao, Y. Ye, Y. Yang, Q. Lin, Z. Zhang, M. O'Keeffe and S. Xiang, Integrating the pillared-layer strategy and pore-space partition method to construct multicomponent MOFs for C_2H_2/CO_2 separation, *J. Am. Chem. Soc.*, 2020, **142**, 9258–9266.
24 Z.-J. Li, Y. Ju, B. Yu, X. Wu, H. Lu, Y. Li, J. Zhou, X. Guo, Z.-H. Zhang, J. Lin, J.-Q. Wang and S. Wang, Modulated synthesis and isoreticular expansion of Th-MOFs with recorded high pore volume and surface area for iodine adsorption, *Chem. Commun.*, 2020, **56**, 6715–6718.
25 Z.-J. Li, Z. Yue, Y. Ju, X. Wu, Y. Ren, S. Wang, Y. Li, Z.-H. Zhang, X. Guo, J. Lin and J.-Q. Wang, Ultrastable thorium metal–organic frameworks for efficient iodine adsorption, *Inorg. Chem.*, 2020, **59**, 4435–4442.
26 R. R. Maldonado, X. Zhang, S. Hanna, X. Gong, N. C. Gianneschi, J. T. Hupp and O. K. Farha, Squeezing the box: isoreticular contraction of pyrene-based linker in a Zr-based metal–organic framework for Xe/Kr separation, *Dalton Trans.*, 2020, **49**, 6553.
27 Y. Tao, Y. Fan, Z. Xu, X. Feng, R. Krishna and F. Luo, Boosting selective adsorption of Xe over Kr by double-accessible open-metal site in metal–organic framework:experimental and theoretical research, *Inorg. Chem.*, 2020, **59**, 11793–11800.
28 K. B. Idrees, Z. Chen, X. Zhang, M. R. Mian, R. J. Drout, T. Islamoglu and O. K. Farha, Tailing pore aperture and structural defects in zirconium-based metal–organic frameworks for krypton/xenon separation, *Chem. Mater.*, 2020, **32**, 376–3782.
29 L. Li, L. Guo, Z. Zhang, Q. Yang, Y. Yang, Z. Bao, Q. Ren and J. Li, A robust squarate-based metal–organic framework demonstrates record-high affinity and selectivity for xenon over krypton, *J. Am. Chem. Soc.*, 2019, **141**, 9358–9364.
30 X.-L. Xiong, G.-H. Chen, S.-T. Xiao, Y.-G. Ouyang, H.-B. Li and Q. Wang, New discovery of metal–organic framework UTSA-280: Ultrahigh adsorption selectivity of krypton over xenon, *J. Phys. Chem. C*, 2020, **124**, 14603–14612.
31 A. Monpezat, S. Topin, L. Deliere, D. Farrusseng and B. Coasne, Evaluation methods of adsorbents for air purification and gas separation at low concentration: case studies on xenon and krypton, *Ind. Eng. Chem. Res.*, 2019, **58**, 4560–4571.
32 Y. Wang, W. Liu, Z. Bai, T. Zheng, M. A. Silver, Y. Li, Y. Wang, X. Wang, J. Diwu, Z. Chai and S. Wang, Employing an unsaturated Th^{4+} site in a porous thorium-organic framework for Kr/Xe uptake and separation, *Angew. Chem., Int. Ed.*, 2018, **57**, 5783–5787.

33 S. Xiong, Y. Gonga, S. Hua, X. Wu, W. Li, Y. He, B. Chen and X. Wang, A microporous metal–organic framework with commensurate adsorption and highly selective separation of xenon, *J. Mater. Chem. A*, 2018, **6**, 4752–4758.

34 Y. Gong, Y. Tang, Z. Mao, X. Wu, Q. Liu, S. Hu, S. Xiong and X. Wang, Metal–organic framework derived nanoporous carbons with highly selective adsorption and separation of xenon, *J. Mater. Chem. A*, 2018, **6**, 13696.

35 H. Bunzen, F. Kolbe, A. Kalytta-Mewes, E. Brunner and D. Volkmer, Achieving large volumetric gas storage capacity in metal–organic frameworks by kinetic trapping: a case study of xenon loading in MFU-4, *J. Am. Chem. Soc.*, 2018, **140**, 10191–10197.

36 J. Li, L. Huang, X. Zou, A. M. Zheng, H. Li, H. Ronga and G. Zhua, Porous organic materials with ultra-small pores and sulfonic functionality for xenon capture with exceptional selectivity, *J. Mater. Chem. A*, 2018, **6**, 11163–11168.

37 P. Zarabadi-Poor and R. Marek, In silico study of (Mn, Fe, Co, Ni, Zn)-BTC metal–organic frameworks for recovering xenon from exhaled anesthetic gas, *ACS Sustainable Chem. Eng.*, 2018, **6**, 15001–15006.

38 Q. Wang, T. Ke, L. Yang, Z. Zhang, X. Cui, Z. Bao, Q. Ren, Q. Yang and H. Xing, Separation of Xe from Kr with record selectivity and productivity in anion-pillared ultramicroporous materials by inverse size-sieving, *Angew. Chem., Int. Ed.*, 2020, **59**, 3423–3428.

39 X. L. Wu, Z. J. Li, H. Zhou, G. Yang, X. Y. Liu, N. Qian, W. Wang, Y. S. Zeng, Z. H. Qian, X. X. Chu and W. Liu, Enhanced adsorption and separation of xenon over krypton *via* an unsaturated calcium center in a metal–organic framework, *Inorg. Chem.*, 2021, **60**, 1506–1512.

40 J. Liu, C. A. Fernandez, P. F. Martin and P. K. Thallapally, A two-column method fot the separation of Kr and Xe from process off-gases, *Ind. Eng. Chem. Res.*, 2014, **53**, 12893–12899.

41 J. Liu, P. K. Thallapally and D. Strachan, Metal–organic frameworks for removal of Xe and Kr from nuclear fuel reprocessing plants, *Langmuir*, 2012, **28**, 11584–11589.

42 S. K. Elsaidi, M. H. Mohamed, C. M. Simon, E. Braun, T. Pham, K. A. Forrest, W. Xu, D. Banerjee, B. Space, M. J. Zaworotko and P. K. Thallapally, Effect of ring rotation upon gas adsorption in SIFSIX-3-M (M=Fe, Ni) pillared square grid networks, *Chem. Sci.*, 2017, **8**, 2373–2380.

43 S. K. Elsaidi, M. H. Mohamed, A. S. Helal, G. Mitchell, T. Pham, S. Suepaul, B. Space, D. Hopkinson, P. K. Thallapally and J. Li, Radiation-resistant metal–organic framework enables efficient separation of krypton fission gas from spent nuclear fuel, *Nat. Commun.*, 2020, **11**, 3103.

44 Z. Yan, Y. Gong, B. Chen, X. Wu, Q. Liu, L. Cui, S. Xiong and S. Peng, Methyl functionalized Zr-Fum MOF with enhanced Xenon adsorption and separation, *Sep. Purif. Technol.*, 2020, **239**, 116514.

45 S. J. Lee, T. U. Yoon, A. R. Kim, S. Y. Kim, K. H. Cho, Y. K. Hwang, J. W. Yeon and Y. S. Bae, Adsorption separation of xenon/krypton mixtures using a zirconium-based metal–organic framework with high hydrothermal and radioactive stabilities, *J. Hazard. Mater.*, 2016, **320**, 512–520.

46 F. Huang, F. Yi, Z. Wang and H. Li, Sorptive removal of Ce(IV) from aqueous solution by bentonite, *Procedia Environ. Sci.*, 2016, **31**, 408–417.

47 Q. Han, M. Du, Y. Guan, G. Luo, Z. Zhang, T. Li and Y. Ji, Removal of simulated radioactive cerium(III) based on innovative magnetic trioctylamine-polystyrene composite microspheres, *Chem. Phys. Lett.*, 2020, **741**, 137092.

48 E. A. Abdel-Galil, R. S. Hassan and M. A. Eid, Assessment of nano-sized stannic silicomolybdate for the removal of ^{137}Cs, ^{90}Sr, and ^{141}Ce radionuclides from radioactive waste solutions, *Appl. Radiat. Isot.*, 2019, **148**, 91–101.

49 G. M. Sheldrick, SHELXT - Integrated space-group and crystal-structure determination, *Acta Crystallogr., Sect. A: Found. Adv.*, 2015, **71**, 3–8.

50 G. M. Sheldrick *SHELXS-97 and SHELXL-97, Program for X-ray Crystal Structures Solution and Refinement*. University of Göttingen, Germany, 1997.

51 O. V. Dolomanov, L. J. Bourhis, R. J. Gildea, J. A. K. Howard and H. Puschmann, OLEX2: a complete structure solution, refinement and analysis program, *J. Appl. Crystallogr.*, 2009, **42**, 339–341.

52 B. J. Sikara, C. E. Wilmer, M. L. Greenfield and R. Q. Snurr, Thermodynamic analysis of Xe/Kr selectivity in over 137000 hypothetical metal–organic frameworks, *Chem. Sci.*, 2012, **3**, 2217–2223.

53 C. M. Simon, R. Mercado, S. K. Schnell, B. Smit and M. Haranczyk, What are the best materials to separate a Xenon/Krypton mixture, *Chem. Mater.*, 2015, **27**, 4459–4475.

54 T. V. Heest, S. L. Teich-McGoldrick, J. A. Greathouse, M. D. Allendorf and D. S. Sholl, Identification of metal–organic framework materials for adsorption separation of rare gases: applicability of ideal adsorbed solution theory (IAST) and effects of in accessible framework regions, *J. Phys. Chem. C*, 2012, **116**, 13183–13195.

55 P. K. Thallapally, J. W. Grate and R. K. Motkuri, Facial xenon capture and release at room temperature using a metal–organic framework: a comparison with activated charcoal, *Chem. Commun.*, 2012, **48**, 347–349.